Visual Clues in Multimodal Rendering

Dani Tost, Anna Puig and Maria Ferré
UPC Software Dept.
URV CS and Math Dept.

May 22, 2002

Abstract

This report presents a comparative analysis of different multimodal rendering methods proposed in [FPT02]. It shows how relevant features of a property as well as relationships between data can be outlined by choosing an appropriate fusion modality. In addition, it analyses the visual clues that can be provided by using different shading models and by enabling rendering parameters such as depth cueing and light source attenuation. The simulations are performed on the software Hipo whose design is described in [PTF02].

1 Introduction

Multimodal rendering consists of visualizing simultaneously various properties of the same 3D region, measured with different registration devices or at different instants of time. The development of measurement technology increases the demand for this type of rendering in many application fields. As an example, in medical applications, it is often necessary to compare images from CTs, which outline bones, and from MR, which show soft tissues. Similarly, the analysis of functional data obtained with PET or SPECT in relation to MR helps understanding how anatomical pathologies may affect patients'activity.
Most of the literature on multimodal rendering focuses at the integration problem, i.e. the establishment of geometrical correspondences between the different input datasets [vdEPV93],[FT01]. Less effort has been concentrated on adapting monomodal rendering methods to multimodal data [CS99] and on the discussion of how fusion must be done in order to provide meaningful images [ZKS+96] [EKBC96].
In an previous work ([FPT02]), we have proposed a general framework that integrates different multimodal fusion algorithms for aligned voxel models. These methods are suitable for raycasting as well as for splatting and 3D hardware assisted texturing. In [PTF02], the design of a software system able to provide these fusion schemes on different types of multimodal studies (1 byte gray-level value, RGB values, float values..) has been discussed.
This report presents a practical comparative analysis of these different methods for medical data. Our goal is to provide criteria to select the most suitable fusion modality according to the type of multimodal study, to the features that should be outlined and to the affordable rendering time. We have therefore performed

sequences of fusions on different phantom and real multimodal case studies and we have analyzed the rendering cost and the image quality in terms of quantity of information that they convey. These results are presented and discussed in Section 4, after a short description of the rendering methods (Section 2) and the fusion strategies (Section 3). The conclusions of this study are presented in Section 5.

2 Rendering methods

The software used for these simulations [PTF02] provides different modeling schemes and rendering modalities. We herein describe only the ones used in the simulations.
The volume representations used are voxel models. The voxel values can be of different types: 1 byte per voxel, float, RGB and RGBα. For each voxel, a gradient vector can be computed according to three schemes: forward difference (gfwd), backward difference (gbwd) and central difference (gcd).

$$\begin{aligned} gfwd_x &= V_{(i+1)jk} - V_{ijk} \\ gfwd_y &= V_{i(j+1)k} - V_{ijk} \\ gfwd_z &= V_{ij(k+1)} - V_{ijk} \end{aligned}$$

$$\begin{aligned} gbwd_x &= V_{ijk} - V_{(i-1)jk} \\ gbwd_y &= V_{ijk} - V_{i(j-1)k} \\ gbwd_z &= V_{ijk} - V_{ij(k-1)} \end{aligned}$$

$$\begin{aligned} gcd_x &= V_{(i+1)jk} - V_{(i-1)jk} \\ gcd_y &= V_{i(j+1)k} - V_{i(j-1)k} \\ gcd_z &= V_{ij(k+1)} - V_{ij(k-1)} \end{aligned}$$

For scalar property values, the differences are computed using directly the voxel values. For vectorial properties such as RGB and RGBα, either one of the channel is used to compute the gradient (for instance Red Value Gradient), or the gradient calculation is based on the RGB or RGBα norm.
The classification is done on the basis of the voxels values through a look-up table. Three different material types can be defined for a voxel:

- emission (E) + absorption (α)
- surface only (ka, kd, ks, kt, Od, Os, n, μ)
- surface and emission + absorption.

There are two main shading models: *per-value shading* and *illumination shading*. In the former method, scalar property values are used as gray-levels, while RGB properties are mapped directly. The opacity per voxel can be set as a constant parameter *(α attenuation)* or as a constant parameter weighted with the property value *(per-value attenuation)*.

Illumination shading is based on Phong equation extended to fitted surfaces in volumes [Lev88]. The color computed at a point p as it is seen in the viewing direction V is:

$$C_\lambda(p,V) = E_\lambda(p) + Ia_\lambda * ka * Od_\lambda + \sum_{i=1}^{nlights} I_i * (kd * Od_\lambda * N \cdot L_i + ks * Os_\lambda * (R_i \cdot V)^n)$$

$$C_\alpha(p,V) \quad = \quad \alpha + (1 - kt)$$

being $\lambda \in \{\mathrm{R}, \mathrm{G}, \mathrm{B}\}$, I_i the i_{th} light source intensity, L_i the normalized vector from p to the i_{th} light source, R_i its reflected vector with regard to the normal vector N, and $E_\lambda(p)$ the emissivity in p, α its linear attenuation coefficient and kd, ks, kt, Od, Os, n the fitted surface optical properties.
The normal vector N is computed as the gradient vector if at least one of the coordinates of the gradient vector is greater than a minimum value:

$$n_{x,y,z} \quad = \quad g_{x,y,z} iff ming_x \leq g_x \vee ming_y \leq g_y \vee ming_z \leq g_z \tag{1}$$

Finally, *Illumination shading* can be modulated by applying depth-cueing, i.e. scaling the computing intensity with the relative depth (z) of the point between two given planes ($zmin$, $zmax$).

$$I_{depthcued} = I * (z - zmin)/(zmax - zmin) \tag{2}$$

Light source attenuation on a point located at distance d from the light source can be defined using a 2nd order polynomial with coefficients a, b, c:

$$I_{attenuated} = \frac{I}{(a * d^2 + b * d + c)} \tag{3}$$

Two different rendering strategies have been tested in this work: raycasting and splatting. In the former method, a set of at least one visibility ray per image pixel is cast through the volume. Samples are taken along the rays either at constant distance or adaptively. In the tests presented herein, the distance is constant. The volume property value at the sample points is computed as the value of the voxel to which the sample belongs or by linear interpolation of the voxel's vertices values. Similarly, the gradient vector can be computed as a constant vector or interpolated. It is assumed that the emission and the absorption are constant between two consecutive samples and that the attenuation between two samples is linear. Being x the distance from the ray origin of a sample point p and being $E(x)$ and $\alpha(x)$ the emission and absorption at p:

$$I(x + \Delta x) \quad = \quad (I(x) + E(x)) * (1 - \Delta x * \alpha(x)) \tag{4}$$

Rays can be integrated Back-to-Front (BTF) as well as Front-to-Back (FTB). In the FTB approach an early termination criterion can be applied: light integration stops as soon as maximum opacity level (1.0) has been reached.

Splatting consists of a sorted traversal of the volume model, either by sheets perpendicular to the viewing direction or voxel-to-voxel. Three different types of splatts can be applied: 1 pixel per voxel, a rectangular constant projection area or a circular or gaussian filter. The splatts are precomputed when loading the voxel rendering preferences and applied during rendering. Two types of traversals are provided: BTF and FTB. No early termination strategy has yet been implemented for splatting, thus the computational times presented in the next sections account for a complete traversal of the model, although only voxels that are projected in the viewport actually pass through the rendering pipeline.

3 Fusion methods

This report addresses 3D fusion methods. An alternative to these methods is the bi-dimensional fusion of final or intermediate images of the two models. An example of bi-dimensional fusion is included in the simulations.
Fusion can occur at different steps of the 3D rendering pipeline: fusion of properties, of materials, within shading computations and of shaded RGBα values. Moreover, the first method, fusion of properties, can take into account only property values or property and gradient values. Therefore, five different pipelines can be defined: Property Fusion (PF), Property and Gradient Fusion (P&F), Material Fusion (MF) Shading Fusion (SF) and Color Fusion (CF).
Besides, two different 3D fusion modalities have been defined:

- selection of one property per point (OPP)
- weighted averaging of properties (MPP)

The OPP scheme is implemented as a decision function that, given combination of input values v_i selects only one of them.

$$f_{opp}(v_1, v_2, .., v_n) \quad = \quad i, 1 \leq i \leq n \tag{5}$$

The value used to render the point is then: $v = v_i$. The OPP scheme can be applied on multimodal studies composed of different types of properties. Once a value has been selected, the rendering pipeline uses it and proceeds as a monomodal pipeline.
The MPP scheme decision function returns n weights w_i, one for each input value, such that $\sum_{i=1}^{n} w_i = 1.0$:

$$f_{mpp}(v_1, v_2, .., v_n) \quad = \quad (w_1, w_2, ..w_n) \tag{6}$$

The rendered value is: $v = \sum_{i=1}^{n} w_i * v_i$. Obviously, the MPP scheme is only applicable on multimodal studies composed of volumes with same property type. Once a new value has been computed, the rendering pipeline continues applying the weighs to its subsequent phases.
The decision functions can be specific ones such as selection of the maximum value for instance, or driven by value range combinations look up tables.
Combining the two modalities and five pipelines, nine fusion methods can be defined:

- PF-OPP: Property fusion (PF) and OPP scheme.
- PF-MPP: Property fusion (PF) and MPP scheme.
- P&GF-OPP: Property and Gradient Fusion (P&GF) and OPP scheme.
- P&GF-MPP: Property and Gradient Fusion (P&GF) and MPP scheme.
- MF-OPP: Material Fusion (MF) and OPP scheme.
- MF-MPP: Material Fusion (MF) and MPP scheme.
- SF-MPP: Shade Fusion (SF) and MPP scheme.
- CF-OPP: Color Fusion (CF) and OPP scheme.
- CF-MPP: Color Fusion (CF) and MPP scheme.

Empirical results of these nine methods are next described.

4 Simulations on Phantom Models

4.1 Phantom models

The phantom models simulate a CT, MR and SPECT study of the human brain. They permit to analyze the accuracy of the different methods without segmentation and noise problems. As the data distribution is deliberately set to provide a division of the 3D volume into known regions, the desired fusion effects can be predicted and compared with the actual ones.
The different models represent a 3D region of 128*128*128. Phantom-CT and Phantom-MR data have 1-byte gray value property while Phantom-SPECT has RGB 1 byte per channel values. The Phantom-CT data distribution consists of two concentrical spheres, one representing the skull and the internal one the brain. Both regions are centered at the voxel (64, 64, 64). Their radii are respectively 52 and 60. The values vary randomly from 60 to 110 in the internal region and from 200 to 250 in the external one. The classification subdivides the external region into two sets: the external one of width 4 and the most internal one that represents the interface between skull and brain.
The Phantom-MR data distribution consists of four regions: a sphere centered at voxel (64, 64, 64) with radius 51 and constant values of 50, a smaller sphere concentrical to the previous one of radius 25 and value 20 and, finally, two small spheres centered at (39, 89, 649) and (89, 89, 64) respectively, with radius 10 and 12.
Finally, the Phantom-SPECT is composed of two symmetrical regions centered at voxel (64, 64, 64) that represent two activity hemispheres with an external radius of 51 and an internal radius of 15. The RGB value within these two regions vary as follows: R(40-50), G(50-60), B(150-250) in the felt hemisphere and R(50-60), G(100-200), B(60-100) in the right one. In addition, there are two internal spherical regions that coincide with the MR small spheres. The left one has values of R(150-255), G=B=50 while the right one values are: R(150-200) G(10-80), B(10-80). The values between ranges are generated randomly.

4.2 Rendering parameters

All simulations have been done using the same final image resolution (500x500). The following parameters have been varied:

- The rendering algorithm (splatting/raycasting).
- The type of shading (per-value or illumination).
- The flag of early termination (ET), only for raycasting.
- The interpolation flag (IT). It indicates if constant values or interpolation values have been used in sampling. It is only for raycasting.
- The type of transparency computation (Transp): it is proportional to the voxel value multiplied by a constant α *(value)* or it is constant *(α)*, set to α . This flag is applied only for value shading.
- The light source attenuation flag (At), only for illumination shading.
- The type of optical property applied: surface only (SO), volume only (VO) or surface and volume (SV).
- The depth-cueing flag (Depth).
- The type of integration FTB or BTF.
- The size of the volume set measured in terms of number of slices of the model that have been rendered.
- The CPU time measured in seconds using the clock function of the standard C time library.

In the tables included below the constant parameters are first described and only the variable ones are enumerated in the tables. The corresponding color plates are referenced in the tables. When the ratio voxel/pixel is low (about 2), as it is the case in many of the simulations, raycasting images and zbuffer images are very similar therefore, only one of the two images generated with the two methods is included.

4.3 Simulations with Phantom-CT

Four simulations sequences have been realized on Phantom-CT data: per-value shading (Table 1) and illumination shading by rendering only surface voxels (Table 2), only voxels interior to a structure (Table 3) and both types of voxels (Table 4).
Figures corresponding to the first simulations are from Figure 1 to Figure 5. Figures 6 and 7 correspond to illumination shading with surface only optical parameters. Finally, 8 shows illumination shading with volume only optical parameters while 9 shows all types of voxels.

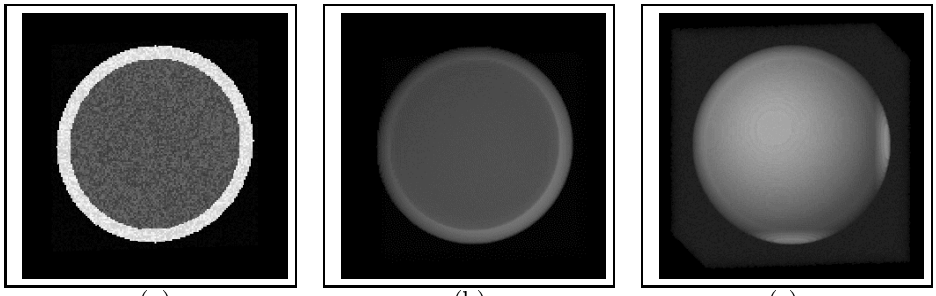

(a) (b) (c)

Figure 1: FTB Images of 1, 64 and 126 slices of the CT data set rendered with raycasting using constant sampling, early termination and no depth-cueing.

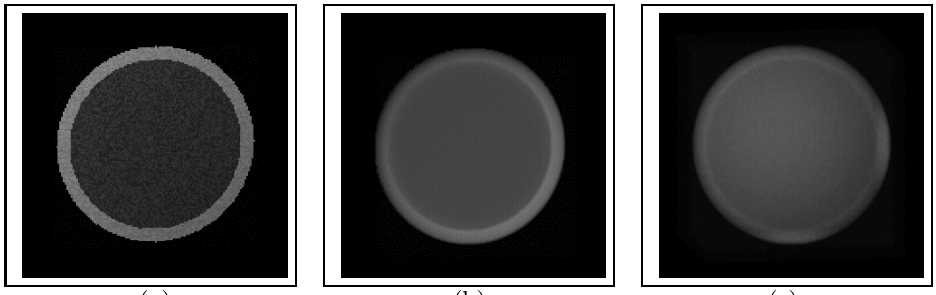

(a) (b) (c)

Figure 2: BTF Images of 1, 64 and 126 slices of the CT data set rendered with splatting using depth-cueing.

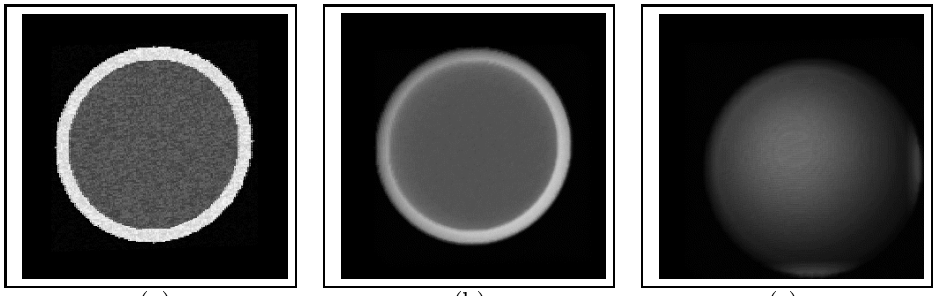

(a) (b) (c)

Figure 3: FTB Images of 1, 64 and 126 slices of the CT data set rendered with raycasting using interpolated sampling and no depth-cueing.

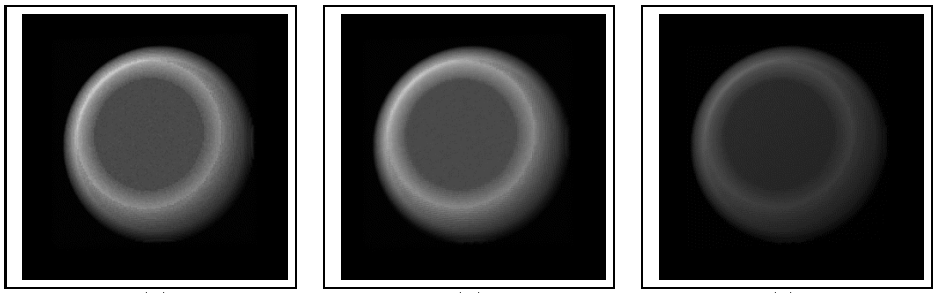

(a) (b) (c)

Figure 4: FTB Images of 40 slices,from 64 to 103, of the CT data set rendered with raycasting using (a) constant sampling and no depth-cueing, (b) interpolated sampling and no depth-cueing (c) interpolated sampling and depth-cueing.

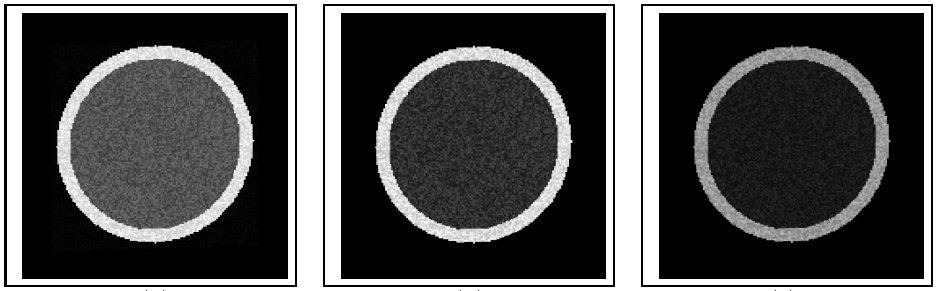

(a) (b) (c)

Figure 5: FTB Images of 1 slice of the CT data set with: (a) constant opacity (b) value opacity*1.0 (c) value opacity*0.5.

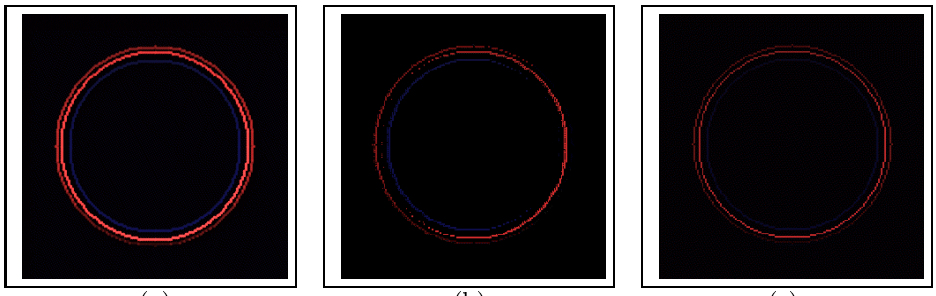

(a) (b) (c)

Figure 6: Images of 1 slice of the CT data set rendered with illumination shading using only surface voxels (a) BTF with interpolated sampling and no depth-cueing, (b) FTB using early termination with interpolated sampling and depth-cueing and (c) FTB using early termination, constant sampling and depth-cueing.

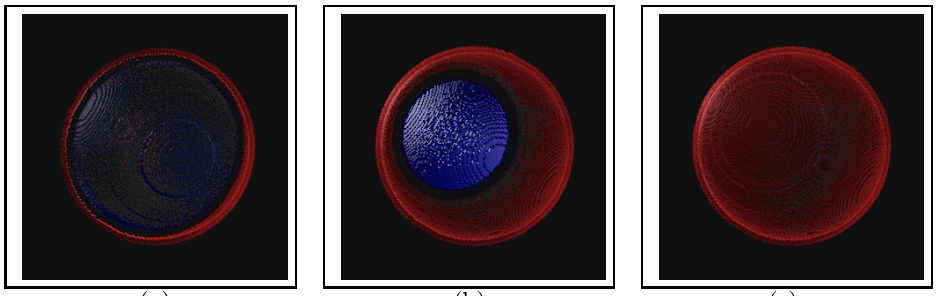

(a) (b) (c)

Figure 7: Images of 64, 103 and 126 slices of the CT data set rendered with FTB raycasting and illumination shading using only surface voxels, applying early termination, constant sampling and depth-cueing.

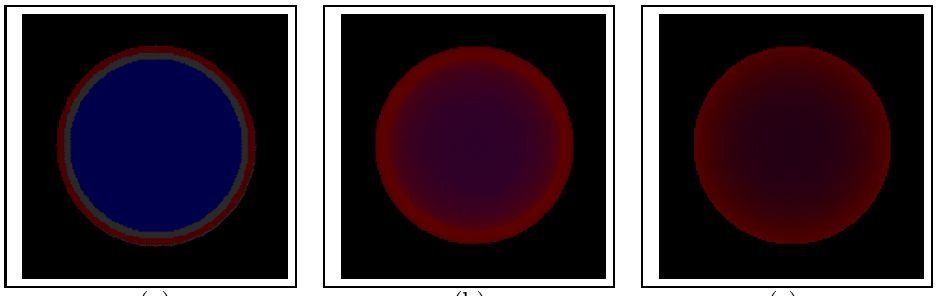

(a) (b) (c)

Figure 8: Images of 1, 64 and 126 slices of the CT data set rendered with FTB raycasting and illumination shading on interior voxels only applying early termination, constant sampling and depth-cueing.

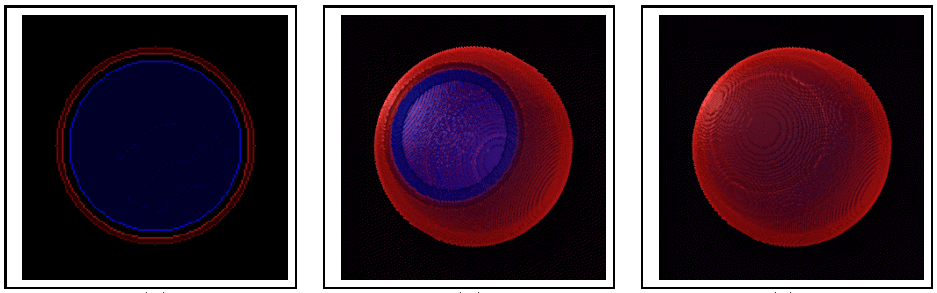

(a) (b) (c)

Figure 9: Images of 1, 103 and 126 slices of the CT data set rendered with FTB raycasting and illumination shading on all voxels applying early termination, constant sampling and depth-cueing.

Algorithm	ET	IT	Depth	Transp	Alpha	Size	Time	Color Plate
Splatting		NO	NO	value	1.0	126x126x1	0.58	
Splatting		NO	NO	alpha	1.0	126x126x1	0.61	
Splatting		NO	NO	alpha	0.5	126x126x1	0.61	
Splatting		NO	YES	value	1.0	126x126x1	0.63	Fig 2a
Splatting		NO	YES	alpha	1.0	126x126x1	0.61	
Splatting		NO	YES	alpha	0.5	126x126x1	0.62	
Raycasting	YES	NO	NO	value	1.0	126x126x1	14.59	Fig 1a 5a
Raycasting	NO	YES	NO	value	1.0	126x126x1	14.96	Fig 3a
Raycasting	YES	NO	NO	alpha	1.0	126x126x1	15.68	Fig 5b
Raycasting	YES	NO	NO	alpha	0.5	126x126x1	15.72	Fig 5c
Raycasting	YES	NO	YES	value	1.0	126x126x1	14.52	
Raycasting	YES	NO	YES	alpha	1.0	126x126x1	15.74	
Raycasting	YES	NO	YES	alpha	0.5	126x126x1	15.84	
Splatting		NO	NO	alpha	0.01	126x126x40	23.52	
Splatting		NO	YES	alpha	0.01	126x126x40	24.11	
Raycasting	YES	NO	NO	alpha	0.05	126x126x40	27.11	Fig 4a
Raycasting	NO	NO	NO	alpha	0.05	126x126x40	27.36	
Raycasting	YES	NO	YES	alpha	0.05	126x126x40	27.68	
Raycasting	NO	NO	YES	alpha	0.05	126x126x40	27.96	
Raycasting	YES	YES	NO	alpha	0.05	126x126x40	84.96	Fig 4b
Raycasting	NO	YES	NO	alpha	0.05	126x126x40	84.99	
Raycasting	YES	YES	YES	alpha	0.05	126x126x40	85.72	Fig 4c
Raycasting	NO	YES	YES	alpha	0.05	126x126x40	85.64	
Splatting		NO	NO	alpha	0.01	126x126x64	36.54	
Splatting		NO	YES	alpha	0.01	126x126x64	36.84	Fig 2b
Raycasting	YES	NO	NO	alpha	0.05	126x126x64	67.60	Fig 1b
Raycasting	NO	NO	NO	alpha	0.05	126x126x64	67.14	
Raycasting	YES	NO	YES	alpha	0.05	126x126x64	68.73	
Raycasting	NO	NO	YES	alpha	0.05	126x126x64	68.72	
Raycasting	YES	YES	NO	alpha	0.05	126x126x64	122.71	
Raycasting	NO	YES	NO	alpha	0.05	126x126x64	123.20	Fib 3b
Raycasting	YES	YES	YES	alpha	0.05	126x126x64	124.52	
Raycasting	NO	YES	YES	alpha	0.05	126x126x64	124.68	
Splatting		NO	NO	alpha	0.01	126x126x126	69.70	
Splatting		NO	YES	alpha	0.01	126x126x126	70.96	Fig 2c
Raycasting	YES	NO	NO	alpha	0.05	126x126x126	116.92	Fig 1c
Raycasting	NO	NO	NO	alpha	0.05	126x126x126	116.70	
Raycasting	YES	NO	YES	alpha	0.05	126x126x126	117.90	
Raycasting	NO	NO	YES	alpha	0.05	126x126x126	117.71	
Raycasting	YES	YES	NO	alpha	0.05	126x126x126	232.93	
Raycasting	NO	YES	NO	alpha	0.05	126x126x126	235.35	Fig 3c
Raycasting	YES	YES	YES	alpha	0.05	126x126x126	234.96	
Raycasting	NO	YES	YES	alpha	0.05	126x126x126	237.62	

Table 1: Phantom-CT Data Simulations with per-value shading.

Algorithm	ET	IT	Depth	Aten.	Rendered values	Size	Time	Color Plate
Splatting		NO	NO	NO	SO	126x126x1	0.37	Fig 6a
Splatting		NO	YES	NO	SO	126x126x1	0.38	
Raycasting	YES	NO	NO	NO	SO	126x126x1	13.91	
Raycasting	YES	NO	YES	NO	SO	126x126x1	13.93	Fig 6c
Raycasting	YES	YES	NO	NO	SO	126x126x1	14.78	
Raycasting	YES	YES	YES	NO	SO	126x126x1	15.05	Fig 6b
Splatting		NO	NO	NO	SO	126x126x64	16.80	
Splatting		NO	YES	NO	SO	126x126x64	18.23	
Raycasting	YES	NO	NO	NO	SO	126x126x64	57.65	
Raycasting	YES	NO	YES	NO	SO	126x126x64	57.63	Fig 7a
Raycasting	YES	YES	NO	NO	SO	126x126x64	90.87	
Raycasting	YES	YES	YES	NO	SO	126x126x64	90.80	
Splatting		NO	NO	NO	SO	126x126x126	34.47	
Splatting		NO	YES	NO	SO	126x126x126	34.79	
Raycasting	YES	NO	NO	NO	SO	126x126x126	59.45	
Raycasting	YES	NO	YES	NO	SO	126x126x126	57.54	Fig 7c
Raycasting	YES	YES	NO	NO	SO	126x126x126	104.34	
Raycasting	YES	YES	YES	NO	SO	126x126x126	103.30	
Raycasting	NO	NO	YES	NO	SO	126x126x126	160.11	
Raycasting	YES	NO	YES	NO	SO	126x126x103	80.63	Fig 7b

Table 2: Phantom-CT Data Simulations with illumination shading and surface-only voxels

Algorithm	ET	IT	Depth	Aten.	Rendered values	Size	Time	Color Plate
Splatting		NO	NO	NO	VO	126x126x1	0.59	
Splatting		NO	YES	NO	VO	126x126x1	0.59	
Raycasting	YES	YES	NO	NO	VO	126x126x1	14.30	
Raycasting	YES	YES	YES	NO	VO	126x126x1	14.27	
Raycasting	YES	NO	NO	NO	VO	126x126x1	13.52	
Raycasting	YES	NO	YES	NO	VO	126x126x1	13.60	Fig 8a
Splatting		NO	NO	NO	VO	126x126x64	26.03	
Splatting		NO	YES	NO	VO	126x126x64	26.46	
Raycasting	YES	NO	NO	NO	VO	126x126x64	81.69	
Raycasting	YES	NO	YES	NO	VO	126x126x64	81.76	Fig 8b
Raycasting	YES	YES	NO	NO	VO	126x126x64	138.10	
Raycasting	YES	YES	YES	NO	VO	126x126x64	140.13	
Splatting		NO	NO	NO	VO	126x126x126	51.34	
Splatting		NO	YES	NO	VO	126x126x126	52.02	
Raycasting	YES	NO	NO	NO	VO	126x126x126	148.69	
Raycasting	YES	NO	YES	NO	VO	126x126x126	146.64	Fig 8c
Raycasting	YES	YES	NO	NO	VO	126x126x126	258.42	
Raycasting	YES	YES	YES	NO	VO	126x126x126	260.10	
Raycasting	NO	NO	YES	NO	VO	126x126x126	145.97	
Raycasting	YES	NO	YES	NO	VO	126x126x103	126.79	

Table 3: Phantom-CT Data Simulations with illumination shading and volume-only voxels

Algorithm	ET	IT	Depth	Aten.	Rendered values	Size	Time	Color Plate
Splatting		NO	NO	NO	VS	126x126x1	0.63	
Splatting		NO	YES	NO	VS	126x126x1	0.64	
Raycasting	YES	NO	NO	NO	VS	126x126x1	18.66	
Raycasting	YES	NO	YES	NO	VS	126x126x1	18.68	Fig 9a
Raycasting	YES	YES	NO	NO	VS	126x126x1	20.38	
Raycasting	YES	YES	YES	NO	VS	126x126x1	20.58	
Splatting		NO	NO	NO	VS	126x126x64	29.44	
Splatting		NO	YES	NO	VS	126x126x64	29.78	
Raycasting	YES	NO	NO	NO	VS	126x126x64	97.22	
Raycasting	YES	NO	YES	NO	VS	126x126x64	101.22	
Raycasting	YES	YES	NO	NO	VS	126x126x64	111.30	
Raycasting	YES	YES	YES	NO	VS	126x126x64	112.32	
Splatting		NO	NO	NO	VS	126x126x126	58.20	
Splatting		NO	YES	NO	VS	126x126x126	58.36	
Raycasting	YES	NO	NO	NO	VS	126x126x126	172.50	
Raycasting	YES	NO	YES	NO	VS	126x126x126	174.63	Fig 9c
Raycasting	YES	YES	NO	NO	VS	126x126x126	125.58	
Raycasting	YES	YES	YES	NO	VS	126x126x126	125.45	
Raycasting	NO	NO	YES	NO	VS	126x126x126	172.83	
Raycasting	YES	NO	YES	NO	VS	126x126x103	152.92	Fig 9b

Table 4: Phantom-CT Data Simulations with illumination shading on all voxels

4.4 Simulation with Phantom-MR

Table 5 shows the parameters of the per-value shading simulations while Table 6 describes the illumination shading simulations. The simulations with illumination shading have been performed using ambient light and three white light sources located on the coordinate axes $+X$, $+Y$, $+Z$ at a distance of 85 from the voxel model center.
Figure 10 shows one slice, half and the whole model using per-value shading. Figure 11 shows variations of the illumination shading by applying light source attenuation, depth-cueing or both. Finally, Figure 12 shows how the illumination shading is affected by the optical properties selected: diffuse colors of the surfaces have been modified and the absorption value varies as (a) low transparency value (0.001) in all structures, (b) medium (0.005), zero in the external structure and (c) 0.005 in the small ones.
Finally, Table 7 shows the simulations results of per-value shading varying the zoom level. Figure 13 represents a zooming detail of the data.

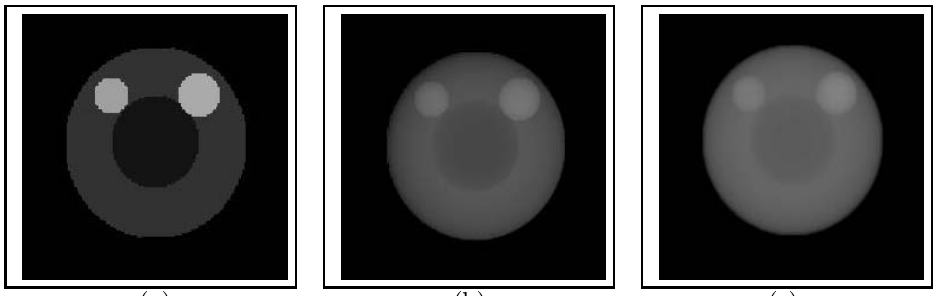

(a) (b) (c)

Figure 10: Images of Phantom-MR data set with per-value shading (a) the middle slice (b) the first half (c) all the model.

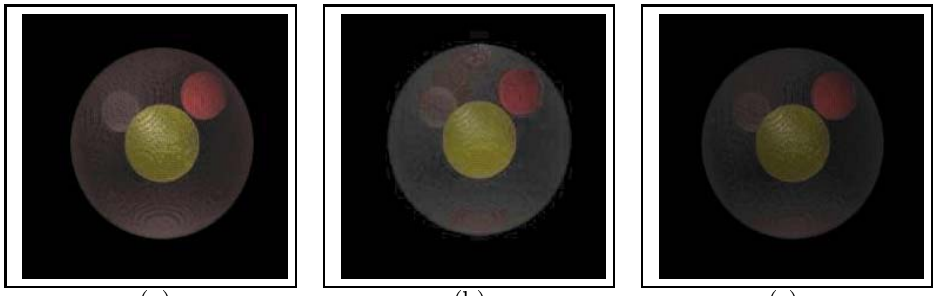

(a) (b) (c)

Figure 11: Images of all the Phantom-MR data set with illumination shading of surface-only voxels, splatting and (a) light source attenuation (b) depth-cueing (c) both light attenuation and depth-cueing.

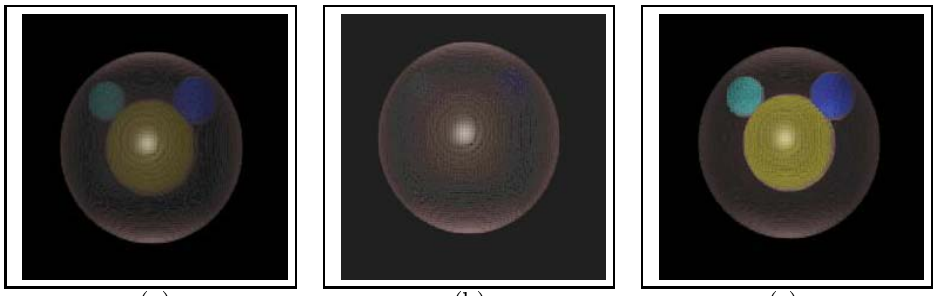

(a) (b) (c)

Figure 12: Images of Phantom-MR data set with illumination shading (a) emission of 0.001 (b) emission of 0.05 (c) emission of 0.05 in the internal structures and 0.0 in the external one.

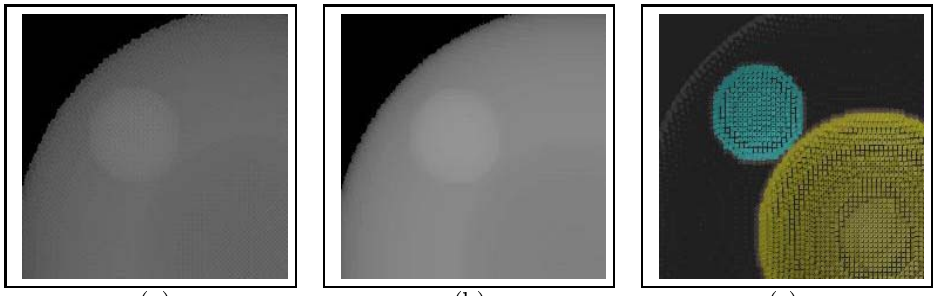

(a) (b) (c)

Figure 13: Zooming detail of the Phantom-MR data set (a) per-value shading with splatting (b) pervalue shading with raycasting and sampling interpolation (c) illumination shading with splatting.

Algorithm	ET	IT	Depth	Transp	Alpha	Size	Time	Color Plate
Raycasting	NO	NO	NO	alpha	1.0	126x126x1	10.52	
Splatting			NO	alpha	1.0	126x126x1	0.44	Fig 10a
Raycasting	YES	NO	NO	alpha	0.01	126x126x64	89.6	
Raycasting	NO	NO	NO	alpha	0.01	126x126x64	89.6	
Splatting			NO	alpha	0.01	126x126x64	18.8	Fig 10b
Raycasting	YES	NO	NO	alpha	0.005	126x126x126	160.7	
Raycasting	NO	NO	NO	alpha	0.005	126x126x126	164.69	
Splatting			NO	alpha	0.005	126x126x126	37.2	Fig 10c

Table 5: Phantom-MR Data Simulations with per value shading

Algorithm	ET	IT	Depth	Aten.	Rendered values	Size	Time	Color Plate
Splatting			NO	NO	SO	126x126x126	23.1	Fig 11a
Splatting			NO	NO	SV	126x126x126	38.8	Fig 11b
Splatting			YES	NO	SO	126x126x126	23.3	
Splatting			YES	NO	SV	126x126x126	38.4	
Splatting			NO	YES	SO	126x126x126	23.5	
Splatting			NO	YES	SV	126x126x126	38.0	
Splatting			YES	YES	SO	126x126x126	24.0	
Splatting			YES	YES	SV	126x126x126	38.1	Fig 11c
Raycasting	NO	NO	NO	NO	SO	126x126x126	85.4	
Raycasting	NO	NO	NO	NO	SV	126x126x126	83.6	
Raycasting	NO	NO	YES	YES	SV	126x126x126	171.9	
Raycasting	NO	YES	YES	YES	SV	126x126x126	318.6	
Raycasting	NO	YES	YES	YES	SV	126x126x126	336.7	

Table 6: Phantom-MR Data Simulations with illumination shading

Algorithm	IT	zoom	Time	Color
Raycasting	NO	1	164.7	Fig 13a
Splatting		1	37.2	
Raycasting	NO	2	758.7	Fig 13b
Raycasting	YES	2	1389.8	
Splatting		2	37.2	Fig 13c

Table 7: Phantom-MR Data Simulations varying the zoom level

4.5 Simulations with Phantom-SPECT model

All the Phantom-SPECT simulations have been performed using per-value shading as Phantom-Spect are directly RGB values.

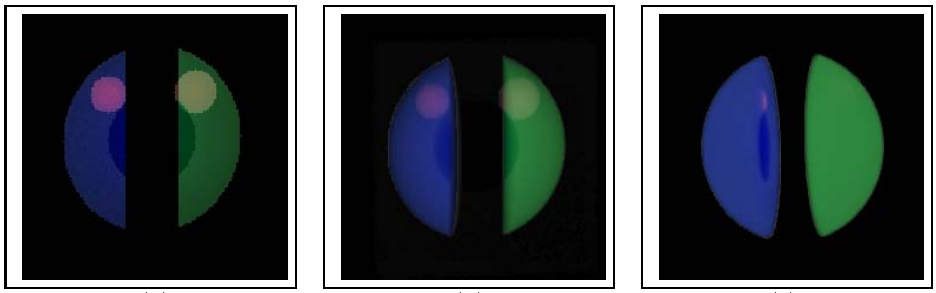

(a) (b) (c)

Figure 14: FTB Images of 1, 64 and 126 slices of the Phantom-SPECTdata set with constant sample and depth-cueing.

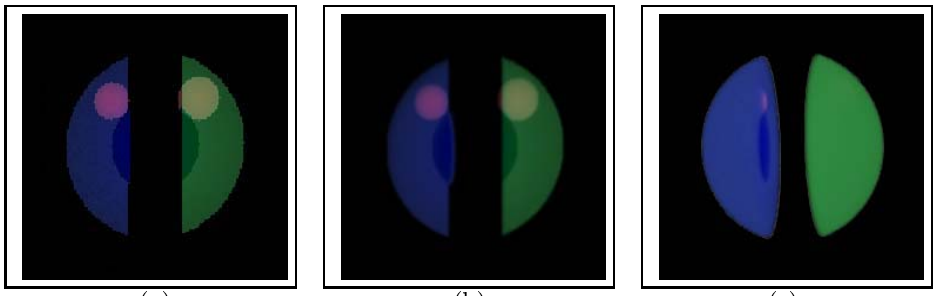

(a) (b) (c)

Figure 15: BTF Images of 1, 64 and 126 slices of the Phantom-SPECT data set with constant sample and depth-cueing.

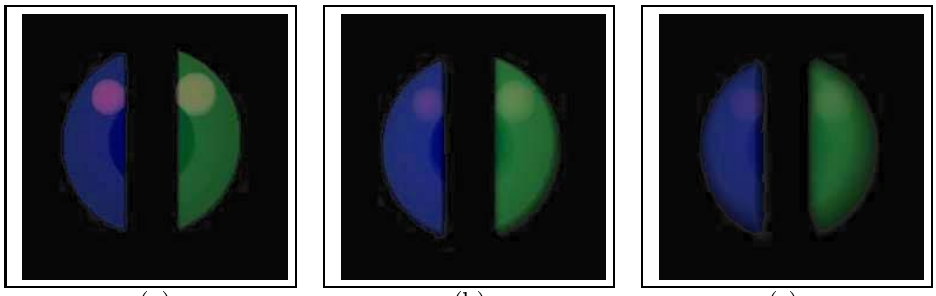

(a) (b) (c)

Figure 16: FTB Images of 10, 30 and 60 slices of the Phantom-SPECT data set with constant sample and depth-cueing.

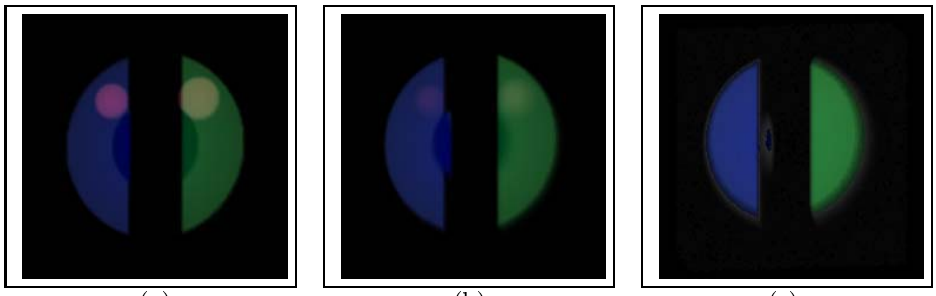

(a) (b) (c)

Figure 17: BTF Images of 10, 30 and 60 slices of the Phantom-SPECT data set with constant sampling and depth-cueing.

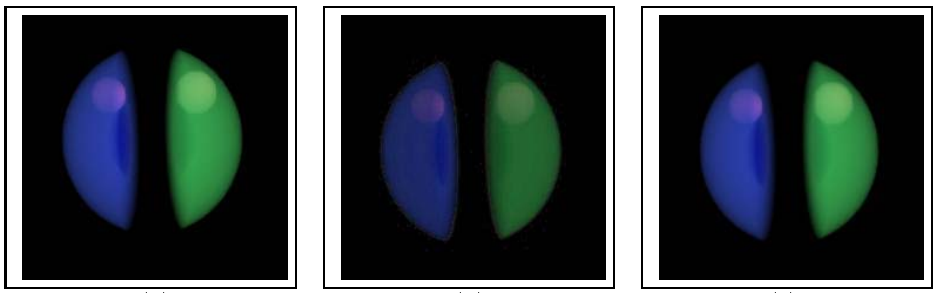

(a) (b) (c)

Figure 18: Images of the Phantom-SPECT data set: (a) constant sampling without depth-cueing, (b) interpolated sampling and depth-cueing, (c) interpolated sampling without depth-cueing.

Algorithm	ET	IT	Depth	Transp	Alpha	Size	Time	Color Plate
Raycasting	YES	NO	YES	alpha	1.0	126x126x1	9.37	Fig 14a
Splatting			YES	alpha	1.0	126x126x1	0.57	Fig 15a
Raycasting	YES	NO	YES	alpha	0.1	126x126x10	11.02	Fig 16a
Splatting			YES	alpha	0.1	126x126x10	6.53	Fig 17a
Raycasting	YES	NO	YES	alpha	0.1	126x126x30	21.45	Fig 16b
Splatting			YES	alpha	0.1	126x126x30	18.50	Fig 17b
Raycasting	YES	NO	YES	alpha	0.05	126x126x60	37.98	Fig 16c
Splatting			YES	alpha	0.05	126x126x60	37.15	Fig 17c
Raycasting	YES	NO	YES	value	0.5	126x126x126	76.12	
Splatting			YES	value	0.5	126x126x126	79.16	Fig 15c
Raycasting	YES	NO	YES	value	0.1	126x126x126	72.67	Fig 14c
Raycasting	YES	NO	NO	value	0.1	126x126x126	78.57	Fig 18a
Raycasting	NO	NO	YES	value	0.1	126x126x126	76.69	
Splatting			YES	value	0.1	126x126x126	79.41	
Raycasting	NO	NO	NO	value	0.1	126x126x126	76.09	
Splatting		NO	NO	value	0.1	126x126x126	77.63	
Raycasting	YES	YES	YES	value	0.1	126x126x126	127.41	
Raycasting	YES	YES	NO	value	0.1	126x126x126	127.26	Fig 18b
Raycasting	NO	YES	YES	value	0.1	126x126x126	128.53	
Raycasting	NO	YES	NO	value	0.1	126x126x126	126.28	Fig 18c

Table 8: Simulations with Phantom-SPECT Data.

4.6 Multimodal Simulations with Phantom-CT and Phantom-MR models

A multimodal study composed of the Phantom-CT model and the Phantom-MR model described before has been constructed. It is aimed at analyzing the possibilities that multimodal rendering offers when it manages modalities that show complementary aspects of the same property. Here, Phantom-CT shows the external structure of the object, equivalent to bone (skull) in real data,and Phantom-MR shows details on the internal structure, equivalent to soft tissue (brain) in the real case.
The simulations present PF-OPP fusions. The criterion used to select the properties is to show high Phantom-CT values (i.e. bone) when present, and MR everywhere else. Two simulations sequences have been realized: per-value shading (Table 9) and illumination shading (Table 10).
The color plate corresponding to the first simulations is Figure 19. Figure 20 corresponds to illumination shading.

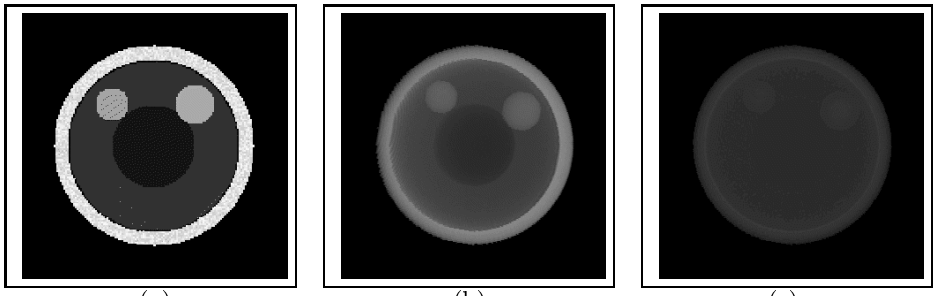

(a) (b) (c)

Figure 19: FTB Images of 1, 64 and 126 slices of the Multimodal CT and MR data set rendered in PF-OPP mode with raycasting using per-value shading, constant sampling, early termination and no depth-cueing.

Algorithm	ET	IT	Depth	Transp	Alfa	Size	Time	Color Plate
Projection		NO	NO	alfa	1.0	126x126x1	0.88	
Projection		NO	YES	alfa	1.0	126x126x1	0.92	
Raytrace	NO	NO	NO	alfa	1.0	126x126x1	14.32	
Raytrace	NO	NO	YES	alfa	1.0	126x126x1	14.40	
Raytrace	NO	YES	NO	alfa	1.0	126x126x1	16.10	
Raytrace	NO	YES	YES	alfa	1.0	126x126x1	16.15	
Raytrace	YES	NO	NO	alfa	1.0	126x126x1	14.37	Fig 19a
Raytrace	YES	NO	YES	alfa	1.0	126x126x1	14.38	
Raytrace	YES	YES	NO	alfa	1.0	126x126x1	16.16	
Raytrace	YES	YES	YES	alfa	1.0	126x126x1	16.07	
Projection		NO	YES	alfa	0.001	126x126x64	43.08	
Raytrace	NO	YES	YES	alfa	0.05	126x126x64	168.94	Fig 19b
Projection		NO	YES	alfa	0.001	126x126x126	90.18	
Raytrace	NO	YES	YES	alfa	0.05	126x126x126	375.11	Fig 19c

Table 9: Multimodal Phantom-CT and Phantom-MR Data Simulations of PF-OPP mode with per-value shading

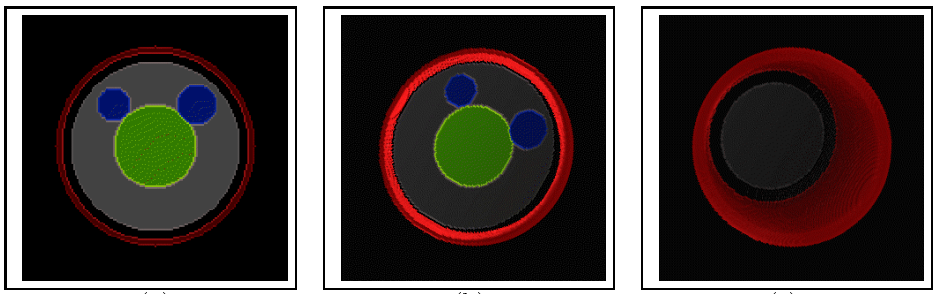

(a) (b) (c)

Figure 20: FTB Images of 1, 64 and 103 slices of the Multimodal CT and MR data set rendered in PF-OPP mode with raycasting using illumination shading, constant sampling, early termination and no depth-cueing.

Algorithm	ET	IT	Depth	Aten.	Rendered values	Size	Time	Color Plate
Raytrace	YES	NO	NO	NO	VS	126x126x1	15.50	Fig 20a
Raytrace	YES	NO	NO	NO	VS	126x126x64	123.80	Fig 20b
Raytrace	YES	NO	NO	NO	VS	126x126x103	187.28	Fig 20c

Table 10: Multimodal Phantom-CT and Phantom-MR Data Simulations of PF-OPP mode with illumination shading

4.7 Multimodal Simulations with Phantom-MR and Phantom-SPECT models

These simulations have been designed to analyze the suitability of the fusion on models which represent different types of properties values, such as density and functionality. The two phantom models are Phantom-MR and Phantom-SPECT described before.
All the Color Plates and simulations presented have been generated using early termination, without depth cueing and without light source attenuation. Color Plates 21 and 22 show the results of a CF-OOP fusion such that only high RGB values from SPECT are displayed and color from MR data are displayed everywhere else. It should be noted that SPECT data are rendered using per-value shading thus, specifying a color value range for SPECT is similar to do a property fusion.
Color Plates 23 and 24 show the results of PF-OOP fusion such that Phantom-SPECT values are displayed whenever they are significant and Phantom-MR everywhere else.

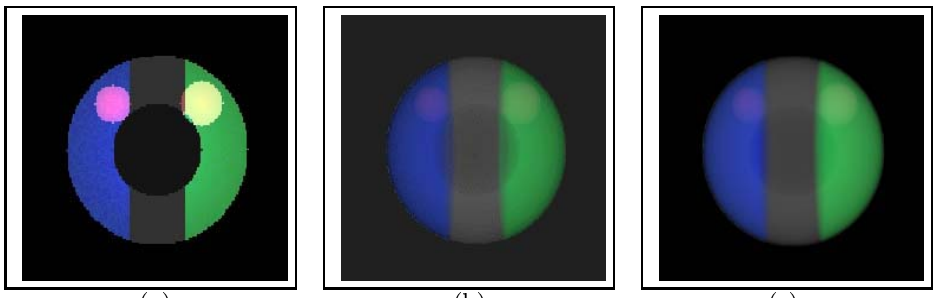

(a) (b) (c)

Figure 21: OOP Color Fusion, using per-value shading (one section, 103 slices and 126 slices).

Color Plate 25 show the differences between the 3D fusion and image fusion: the first two pictures show MR and SPECT monomodal rendering, the third one the multimodal simulation and the last one the sum of images. Again, the quality of 2D fusion is good, because the images show well segmented structures.

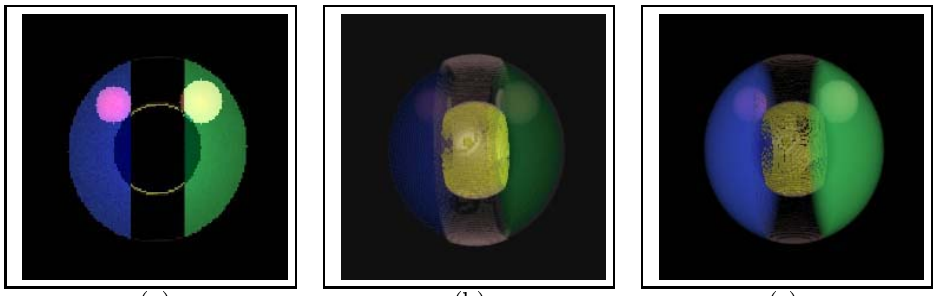

(a) (b) (c)

Figure 22: OOP Color Fusion, using illumination shading of Phantom-MR and per-value shading of Phantom-SPECT (one section, splatting of 126 slices and raycast of 126 slices).

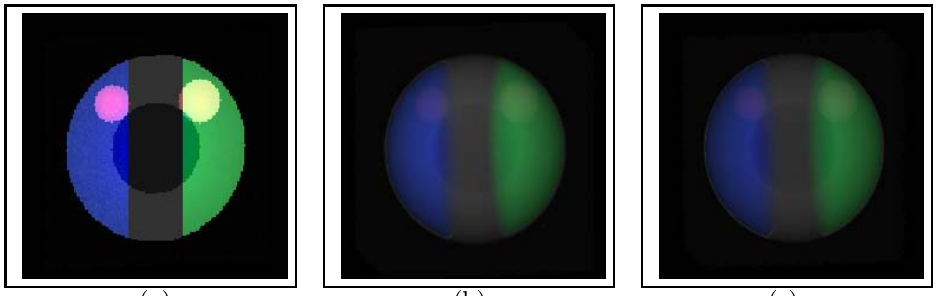

(a) (b) (c)

Figure 23: OOP PropertyFusion (one section, splatting of 126 slices and raycast of 126 slices), using per-value shading for both models.

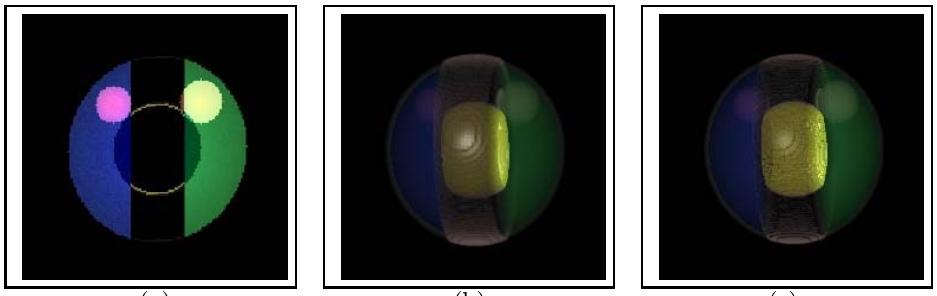

(a) (b) (c)

Figure 24: OOP PropertyFusion (one section, splatting of 126 slices and raycast of 126 slices), using illumination shading for Phantom-MR and per-value shading for Phantom-SPECT.

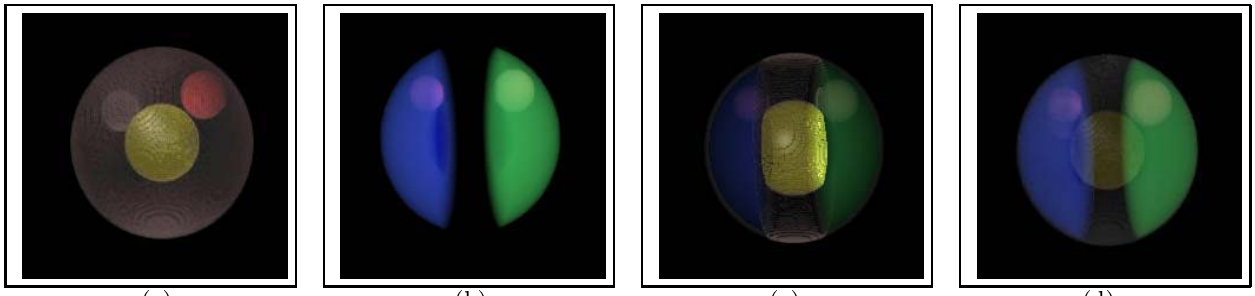

(a) (b) (c) (d)

Figure 25: FTB Images of 1, 64 and 126 slices of the CT data set rendered with raycasting using constant sampling, early termination and no depth-cueing.

Fusion	Type	Criteria	Shade	Algorithm	Size	Time	Color Plate
Color	Index	Red -¿ Spect	Value	Splatting	126x126x1	0.72	Fig 21a
Color	Index	Red -¿ Spect	Value	Raycasting	126x126x1	11.51	Fig 21a
Color	Index	Red -¿ Spect	Value	Raycasting	126x126x103	245.20	Fig 21b
Color	Index	Red -¿ Spect	Value	Splatting	126x126x126	95.95	Fig 21c
Color	Index	Red -¿ Spect	Value	Raycasting	126x126x126	274.91	
Color	Index	Red -¿ Spect	Shade/Value	Splatting	126x126x1	0.84	Fig 22a
Color	Index	Red -¿ Spect	Shade/Value	Raycasting	126x126x1	12.36	Fig 22a
Color	Index	Red -¿ Spect	Shade/Value	Splatting	126x126x126	108.0	Fig 22b
Color	Index	Red -¿ Spect	Shade/Value	Raycasting	126x126x126	311.84	Fig 22c
Property	Index	Spect over Mr	Value/Value	Splatting	126x126x1	0.82	Fig 23a
Property	Index	Spect over Mr	Value/Value	Raycasting	126x126x1	9.76	Fig 23a
Property	Index	Spect over Mr	Value/Value	Splatting	126x126x126	106.58	Fig 23b
Property	Index	Spect over Mr	Value/Value	Raycasting	126x126x126	321.27	Fig 23c
Property	Index	Spect over Mr	Shade/Value	Splatting	126x126x1	0.83	Fig 24a
Property	Index	Spect over Mr	Shade/Value	Raycasting	126x126x1	13.01	Fig 24a
Property	Index	Spect over Mr	Shade/Value	Splatting	126x126x126	110.52	Fig 24b
Property	Index	Spect over Mr	Shade/Value	Raycasting	126x126x126	349.01	Fig 24c
Property	Index	Spect over Mr	Shade/Value	Interpolated raycasting	126x126x126	510.85	

Table 11: Simulations with Phantom-MR and Phantom-SPECT Data.

4.8 Multimodal simulations with two Phantom-MR models

These simulations have been designed to analyze the suitability of the fusion on two slightly different models such as datasets from the same modality but captured at different instants of time or corresponding to two different subjects as for instance, a standard or atlas reference model and a real one. Two Phantom-MR models have been generated, one identical to the one analyzed previously and the other one with the features translated of 4 voxels in the x and y directions.
Color plates 26 show the result of weighted color fusion on one slice, varying the weights.

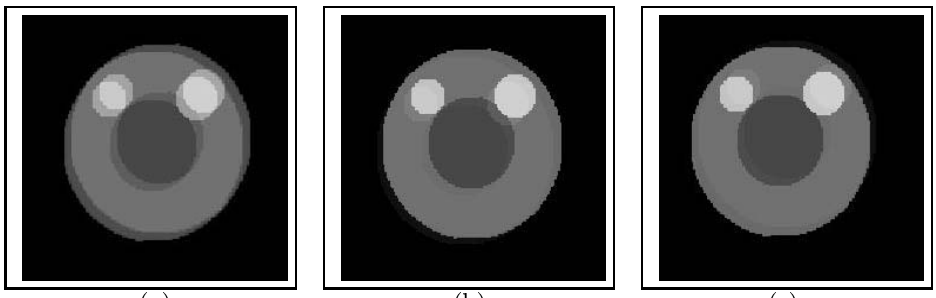

(a) (b) (c)

Figure 26: One slice of the multimodal Phantom MR-MR dataset applying per-value shading and weighted color fusion: (a) weights of 0.5 for each channel and color, (b) weights of 0.9 for the first color and 0.1 for the other one (c) weights of 0.1 for the first dataset and 0.9 for the second one.

Color Plates 27 show the results of per-value shading splatting with PF-OPP on one slice and 126 slices as well as PF-MPP on 126 slices with weight 0.1 and 0.9. Table 12 shows the computational cost of the simulations.

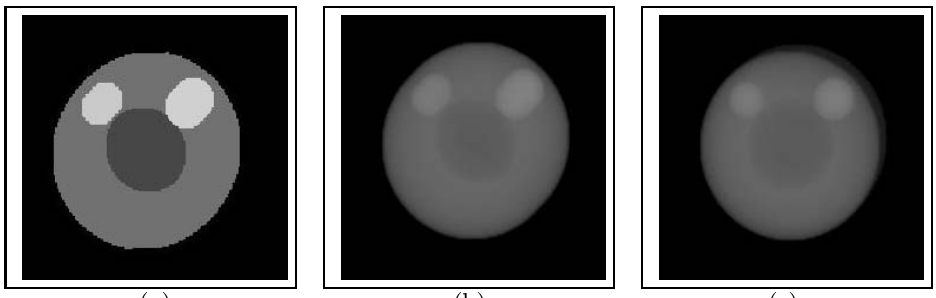

(a) (b) (c)

Figure 27: Property fusion on the multimodal Phantom MR-MR dataset : (a) OPP, 1 slice, (b) OPP 126 slices (c) MPP weights of 0.1 0.9.

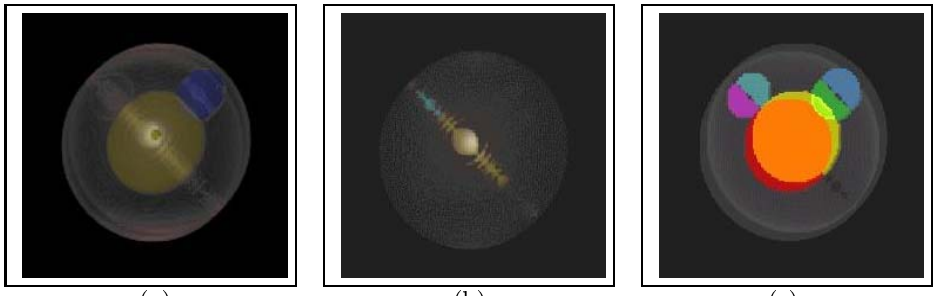

(a) (b) (c)

Figure 28: Fusion modalities on the multimodal Phantom MR-MR dataset : (a) CF-MPP, weights 0.5, (b) PF-MPP weights 05 (c) MF-MPP weights of 0.5 in the commom area.

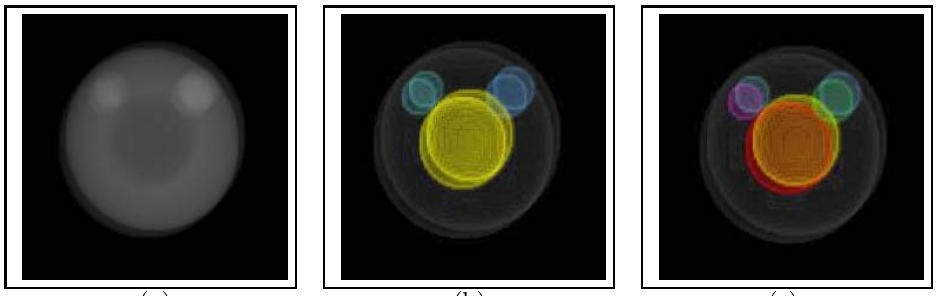

(a) (b) (c)

Figure 29: Average of images resulting from monomodal rendering processes: (a) per-value shading, (b) illumination shading (c) illumination shading with different optical properties per set.

Shading	Rendered values	Fusion	Mode	Size	Time	Color Plate
value		PF	Idx	126x126x126	67.6	Fig 26b
value		PF	Weight	126x126x126	72.1	Fig 26c
illum.	SV	PF	Idx	126x126x126	66.7	
illum.	SV	PF	Weight	126x126x126	85.1	Fig 27b
value		CF	Idx	1b26x126x126	67.6	
value		CF	Weight	126x126x126	74.3	Fig 27a
illum.	SV	CF	Idx	126x126x126	66.7	
illum.	VO	CF	Weight	126x126x126	65.7	
illum	VO	MF	Idx	126x126x126	61.3	Fig 27c

Table 12: Simulations with Phantom-MR and Phantom-MR Data.

Color Plates 28 show the results of illumination shading splatting with weighted color, property and material fusion
Finally, Color Plates 29 show the results of rendering each dataset separately and averaging the resulting images. The quality is surpringly good, because the images are very similar and very well segmented, thus possible 3D occusions that would have been hidden in the image fusion do not exist.

4.9 Simulations with real MR and SPECT models

A real MR model of the brain and an aligned SPECT model have been tested. They have been downloaded from [Hos01]. The model size is 190x220x178. MR data are 1 byte gray values and SPECT 3-byte RGB values. Color plate 30 shows the result of visualizing each dataset.

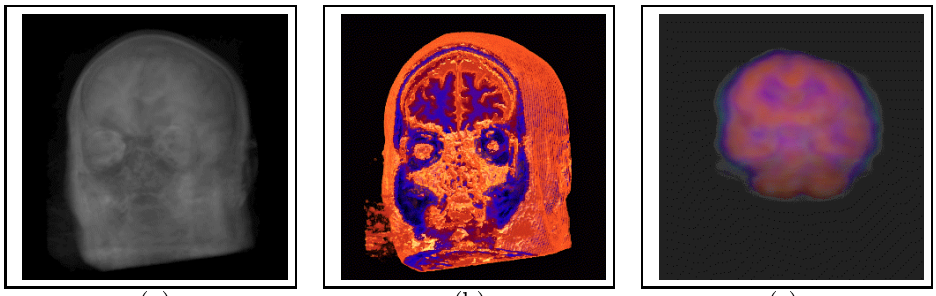

(a) (b) (c)

Figure 30: FTB monomodal images of each dataset: (a) MR dataset applying per-value shading (b) MR dataset applying per-value shading and (c) SPECT dataset applying per-value shading

Color Plates 31 show the results of per-value shading with Property fusion and Property and Gradient Fusion. Because the datasets correspond to different properties only OPP is treated.

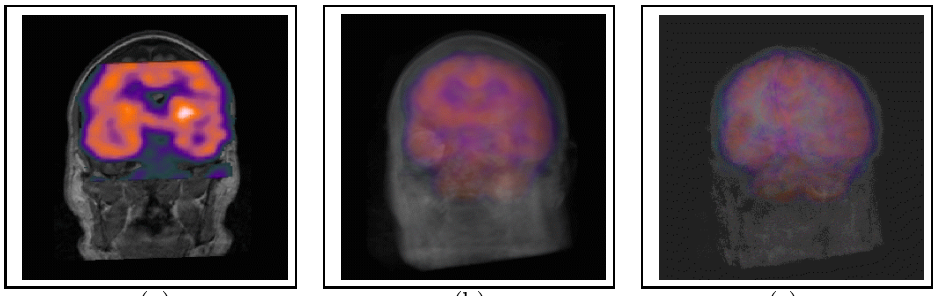

(a) (b) (c)

Figure 31: OPP fusion on the multimodal MR-SPECT dataset : (a) Property Fusion, 1 slice, (b) Property Fusion of 178 slices (c) Property and Gradient Fusion of 178 slices

Color Plates 32 show the results of material fusion strategy. Color Plates 33 show the results of color fusion.

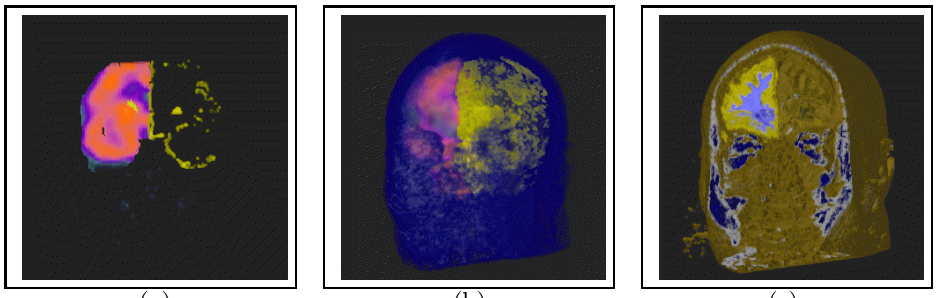

(a) (b) (c)

Figure 32: Material Fusion on the multimodal MR-SPECT dataset : (a) OPP of 1 slice (b) OPP of 178 slices (c) MPP of 146 slices.

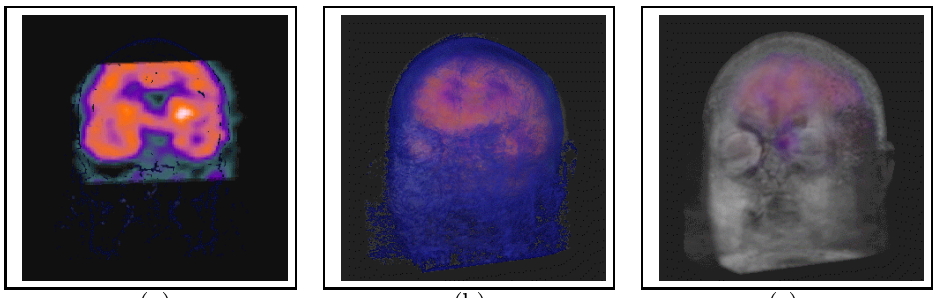

(a) (b) (c)

Figure 33: Color Fusion on the multimodal MR-SPECT dataset : (a) OPP of 1 slice (b) OPP of 178 slices (c) MPP of 178 slices

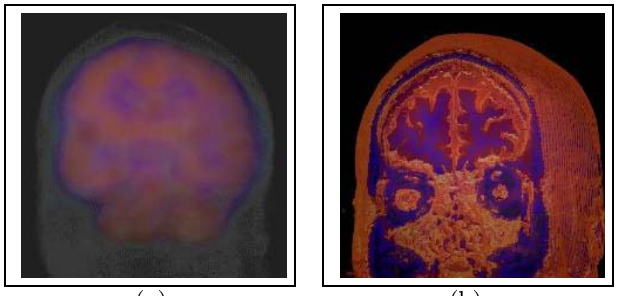

(a) (b)

Figure 34: 2D Fusion of monomodal images of MR and SPECT: (a) per-value shading (b) illumination shading for MR and per-value shading for SPECT.

Shading	Rendered values	Fusion	Mode	Size	Time	Color Plate
value		PF	Idx	190x220x1	2.09	Fig 29a
value		PF	Idx	190x220x178	355.59	Fig 29b
value		P&GF	Idx	190x220x178	458.12	Fig 29c
illum	SV	MF	Idx	190x220x1	2.16	Fig 30a
illum	SV	MF	Idx	190x220x178	349.31	Fig 30b
illum	SV	MF	Weight	190x220x178	444.47	
illum	SV	MF	Weight	190x220x146	362.14	Fig 30c
illum.	SV	CF	Idx	190x220x1	1.68	Fig 31a
illum.	SV	CF	Idx	190x220x178	502.95	Fig 31b
value		CF	Weight	190x220x178	652.01	Fig 31c

Table 13: Simulations with real MR and SPECT Data.

Finally, Color Plate 34 shows the result of the bi-dimensional fusion of images from the two monomodal rendering pipelines. Because of the complexity of the structures, the images give very little visual clues on the multimodal set.

5 Results Analysis

The results presented in the previous section lead to various conclusions, some of them general, attributable to the rendering modalities and other specific of multimodality.

5.1 General results

Shading models

Comparing the two shading models on the phantom models, the color plates show that per-value shading gives a general view of the data while illumination shading enhances the surfaces. Per-value shading may be easily applied on any data. Illumination shading is not suitable for RGB (SPECT) data which already convey the desirable color information.
The major difficulty for per-value shading is the computation of the opacity: too high values give opaque images and too low ones give very dark pictures. Scaling the opacities directly according to the voxel values gives poor adjustments. A constant opacity is easier to fix, starting with an approximation of $1/n$ being n the number of voxels per edge. However, scaling the opacities according to the voxel values and a constant factor seems to give a better perception of the data while keeping low the overall opacity. However, it should be noted that most of the images included in the text have been gamma corrected.
In order to obtain good visual results using illumination shading, it is essential to have a good segmentation of the surfaces and an accurate measure of the minimum gradient value in each direction. Otherwise, for non-homogeneous regions, all voxels may potentially have significant gradient values, which will lead to very opaque images. In the Phantom datasets, the variation between adjacent voxels is low and the value ranges of each region is very different. Therefore, only a limited number of voxels were classified as surface-voxels. In the real MR data, however, the different regions share the same value ranges

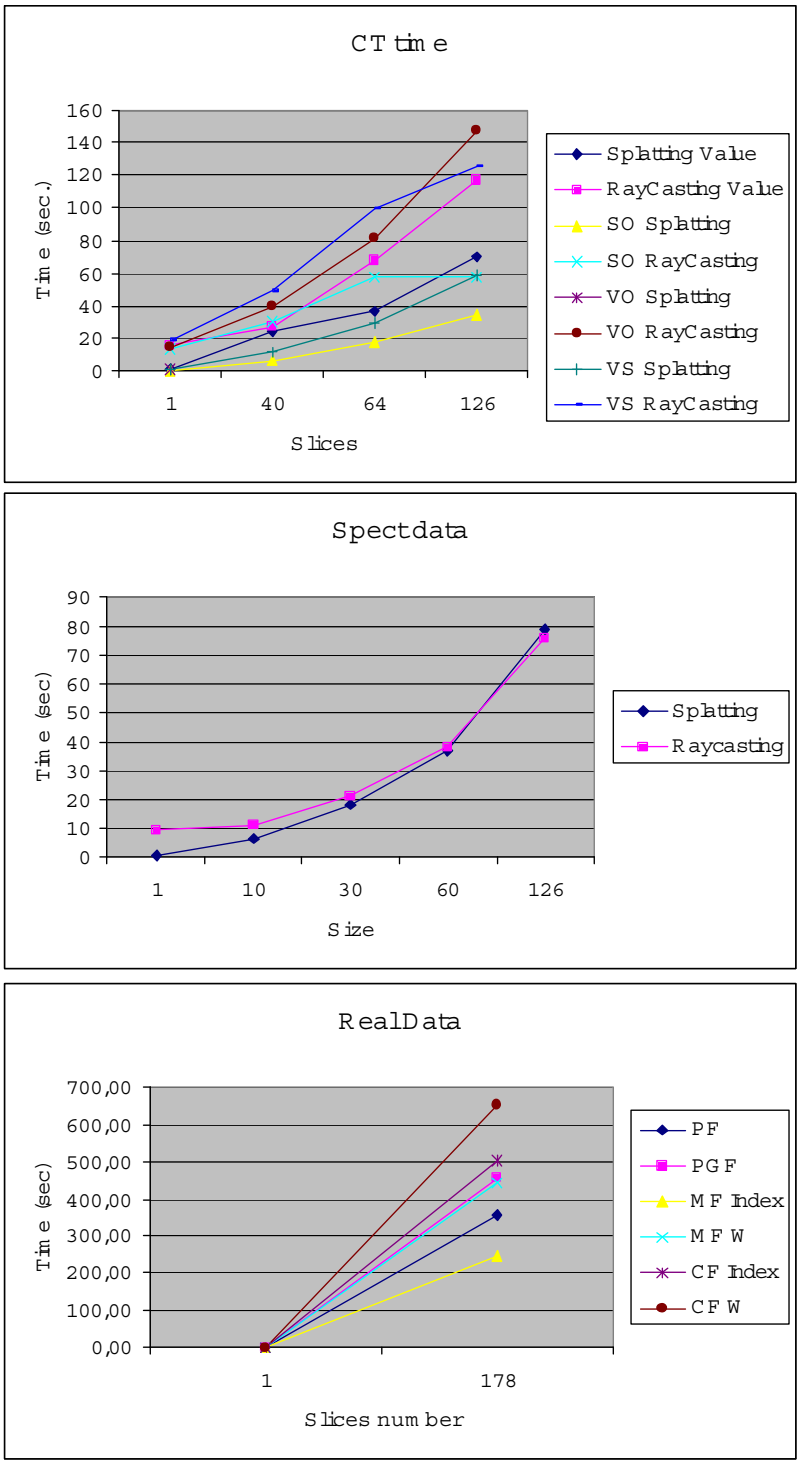

Figure 35: Time evolution in function of slice number with the real data.

and almost all voxels are classified as surface ones. In order to obtain semi-transparent surfaces, the labeled segmented model is needed.
Finally, it is more difficult to match the surfaces with raycasting than with splatting. Thus, the sampling ratio along the rays of illumination shading must be higher than with per-value shading.

Rendering algorithms

The image quality of raycasting images and splatting images is similar in most of the simulations because the ratio voxel/pixel is around 2. However, as shown in pictures 13, zooming with raycasting gives a much better quality than splatting. Square homogeneous spots used as footprint give artifacts such as black lines or overlapping lines for axial views. This can be avoided using gaussian footprints but the cost of the rendering increases because in order to provide smooth enough images these footprints need to be larger (a minimum gaussian footprint size equivalent to a 2x2 homogeneous spot is 3x3, for instance) (see Table 7).
As shown in 8 depth-cueing has a visible impact on the images. For the phantom models, this effect is not always desirable because being symmetrical objects, the 3D structure of the model is rather clear without need of depth-cueing that occludes part of the data. For real data, instead, far high valued samples may appear at the first plane of the image and mislead data interpretation. In this case, depth-cueing is necessary.
Light source attenuation effect is shown in 10. It darkens slightly the images, outlining more or less the surfaces. In the phantom models, because they are perfectly segmented and have a clear boundary, this effect is perceptible. It is instead less important on fuzzier data such as the real ones.

Computational cost

Monomodal simulations on Phantom-CT, Phantom-MR and Phantom-SPECT show that the rendering cost of splatting and raycasting without early termination are proportional to the size of the model rendered. See for instance the evolution of time values according to the size of the CT model plotted in Figure 35 below. The linear dependence appears with all shading models. This result is expectable for splatting because this method traverses the entire model and in these simulations all the voxels fell into the viewport and thus passed through the viewing pipeline. Furthermore, the same effect occurs in raycasting of the whole model without early termination.
The early termination criterion only diminishes the raycasting cost if maximum opacity is reached soon during ray integration. When per-value shading is applied, in order to see the volume as much transparent as possible, very low opacity values were used (around 0.05 for the whole models). Therefore, the early termination criterion was never matched and early termination costs are similar to non-early termination ones. On the contrary, when illumination shading was applied, the criterion was matched soon, at surfaces. Thus, reductions of more than one half of the CPU time are obtained.
Comparing identical simulations on each of three Phantom datasets, it can be seen that Phantom-CT costs are a little higher than Phantom-MR. This is because the occupancy of non-void voxels is higher in Phantom-CT. Phantom-Spect cost are much higher than the two others. This is because the values are RGB, thus its occupancy is three times bigger.
As expected, raycasting is more computationally expensive than splatting, even with a sampling rate of 1 and no interpolation. Increasing the number of samples

per ray makes this difference grow dramatically. Similarly, interpolating sample values can multiply by two the cost of the rendering.
With regards to the shading models, their costs are more or less similar with splatting. However, comparing illumination shading on Phantom-MR (Table 5) with per-value shading using raycasting (Table 6), the cost of the former one is much higher. This is not attributable to the shading process itself but to the fact that the sampling rate has been increased from 1 to 0.5 in order to match the surface.
Finally, neither depth cueing nor light source attenuation increase significantly the computational cost of the rendering.

5.2 Results of multimodality

Modalities

In the different simulations that we have performed, we have tried to show a variety of fusion cases. In some cases, the fusion is intended at outlining in one image features from different modalities such as the skull from CT and the brain with MR or significant SPECT values and MR everywhere else. The OPP mode is the most suitable for this type of rendering, because MPP is only applicable on similar properties and materials. In other cases, such as MR with MR, the fusion is intended at outlining the differences between two similar datasets. The MPP mode is convenient for this case.
In the OPP mode, from a user point of view, the problem is how to specify the features that should be outlined. The simplest way is using a material identifier. Thus, MF-OPP and the SF-OPP seem the best choice. However, these modes are only meaningful on pre-classified data.
PF-OPP is an indirect way for specifying a feature that can be applied on all the datasets. It is simple to specify for users having knowledge of the property value distributions. Nevertheless, when the property values are not restricted to a region this mode can give erroneous results. As an example, MR data values are distributed over the model and it is not possible to select an anatomical structure on the basis of its values.
P&GF brings a useful way to outline the surface of given feature. However, if the range of property values within a region is wide, many samples have a significant gradient value and thus, P&GF will give similar results to PF. The P&GF performed on real data in the simulations, uses the pre-classified model which allows distinguishing internal and boundary voxels. The results of the same simulation on non-classified data were not of interest.
CF-OPP works similarly to PF when per-value shading is used. When illumination shading is used, it is very difficult for the user to predict the expected colors of the features that should be outlined. In the simulations of MR with SPECT, the criterion used is to show SPECT colors whenever they were significant. Thus, the images correctly show high SPECT values and illumination shaded MR structures everywhere else. However, if a range of MR color values is also specified, the images are meaningless, exhibiting in one pixel a high SPECT value and at the next pixel a highlight on a MR surface.
The second type of simulations is the mixture of elements. The simulations with Phantom-MR and Phantom-MR are an example of this. In this case, PF-MPP is simple to apply and it gives a good feedback of the differences between

datasets, especially if several simulations varying the weights are performed. A problem that may appear in data having a high variability of properties within a region is that the average of values can blur the final image which will result meaningless. CF-MPP with per-value shading gives the same results. However, it is difficult to find accurate color range values for illumination shading.
Finally, some simulations of image fusion have been performed with the MR-MR multimodal dataset, the MR-SPECT and the real MR-SPECT. The results on Phantom datasets are surprisingly good, but they are poor with the real set. This is because Phantom datasets have simple and well segmented structures. The complexity of real data makes it difficult to give clues on the relationships between 3D structures in a 2D projection.

Computational cost

As expected, rendering multimodal data increases the CPU time which reaches values of a little more than the sum of the monomodal rendering time of each data set separately. However, having in memory a multimodal data set, do not increase the monomodal rendering cost of one the sets.
In each fusion mode, the pipeline through which data pass is different. Therefore, the cost of each rendering varies. In principle, the further in the pipeline the fusion occurs, the higher is the cost. Thus, from lower to higher the costs should correspond to PF, P&GF, MF, SF and CF. The simulations corroborate this principle although differences between processes are sometimes lower than expected. This is due to the fact that the costs depend also on many other parameters, such as the number of samples which actually pass through one or the other pipeline.
Analyzing the real dataset, for instance, it can be observed that the CPU times for OPP modes follow the expected curve except for MF whose cost is slightly lower than PF (249 versus 355). This is due to the fact that MF was done on a pre-classified MR model with much less significant values than the original one. Using non classified data gives a CPU time of 412, higher than PF.
Comparing OPP and MPP modes, the later one gives higher CPU times. This is due to the weighting process that is applied on property values, gradient vectors and optical properties. In addition, as mentioned before, the MPP is sometimes more difficult to tune and more ranges of values should be specified to assign the different weights, thus, for each sample, more boolean expressions should be evaluated.

6 Conclusions

This report has presented the results of empirical analysis of different rendering strategies and fusion methods. Although many more simulations could be done, we have tried to focus at the most relevant parameters for multimodal rendering, especially oriented at medical images.
The nine fusion methods tested herein have different usage depending on the type of data and the expected results. From a user point of view, material fusion is probably the simplest mode, as it only needs the specification of the material identifier, by opposite to property values or colors. However, it requires an explicit classification process which is not always done, especially when property values are used as indexes to transfer functions. Shading fusion is a variant of weighted material fusion that may tune the relative importance of surfaces.

Nevertheless, it is only distinguishable from material fusion if illumination shading is used and for specific lighting models. Property fusion gives good results on well segmented data but it is difficult to tune on regions having a wide range of property values. Property and gradient fusion is useful to outline surfaces if the data are segmented enough to guarantee that only a small subset of voxels have significant gradient vectors. Color fusion is easy when it mixes models that give separate color ranges, as for instance gray values with RGB values. It is also appropriate for the fusion of data from the same modality. However, its results for other cases are less predictable. Finally, in general, the OPP mode is simpler to use because the estimation of appropriate weights is difficult. A case in which MPP mode has proved to be especially useful is for the fusion of data from the same modality because depending on the weights, it may outline the differences or by the contrary smooth them.
New trends for the future are the design of friendly interfaces that could help users to interactively specify fusion parameters. In addition, open research lines are algorithms able to compute automatically the fusion parameters. Another topic that should be studied is the use of dynamic presentations of multimodal data. Varying the fusion parameters along time would provide more clues on the relationships between data. This is not feasible now, because the computational time of one rendering is high. Therefore, new rendering techniques relying on temporal coherence should be investigated.

References

[CS99] W. Cai and G. Sakas. Data intermixing and multivolume rendering. *Computer Graphics Forum*, 18(3):359–368, 1999.

[EKBC96] N. El-Khalili, K. Brodlie, and W. Crum. Visualization of medical data by volume rendering of ct and spect images. *UK-EG Conference*, pages 283–295, 1996.

[FPT02] M. Ferre, A. Puig, and D. Tost. Rendering techniques for multimodal data. *Report LSI- 64-R*, 2002.

[FT01] M. Ferre and D. Tost. Integration of multimodal data based on surface registration. *Proceedings of METMBS'01*, pages 73–77, June 2001.

[Hos01] Massachusetts General Hospital. Internet brain segmentation repository. http://neuro-www.mgh.harvard.edu/cma/ibsr. *Internet Address*, 2001.

[Lev88] M. Levoy. Display of surfaces from volume data. *IEEE Computer Graphics and Applications*, 8:29–37, May 1988.

[PTF02] A. Puig, D. Tost, and M. Ferre. Design of multimodal system. *Report LSI-37-R*, 2002.

[vdEPV93] P.A. van den Elsen, E.J.D. Pol, and M.A. Viergever. Medical image matching. a review with classification. *IEEE Engineering in Medicine and Biology*, pages 26–39, March 1993.

[ZKS+96] K.J. Zuiderveld, A.H.J. Koning, R. Stokking, J.B.A. Maintz, F.J.R. Appelman, and M.A. Viergever. Multimodality visualization of medical volume data. *Computer and Graphics*, 20(6):775–791, 1996.